University of
BRISTOL

Peer reviewed version

Link to published version (if available):
10.1038/NCHEM.2570

Link to publication record in Explore Bristol Research
PDF-document

University of Bristol - Explore Bristol Research
General rights

Translational, rotational, and vibrational relaxation dynamics of a solute molecule in a non-interacting solvent

Authors: Michael P. Grubb[1,2]*, Philip M. Coulter[1], Hugo J.B. Marroux[1], Balazs Hornung[1], Ryan S. McMullen[1], Andrew J. Orr-Ewing[1], Michael N.R. Ashfold[1]

Affiliations:

[1]School of Chemistry, University of Bristol, Cantock's Close, Bristol BS8 1TS, UK.

[2]Department of Chemistry, Fort Lewis College, Durango, CO 81301.

*Correspondence to: mpgrubb@fortlewis.edu

Abstract: Spectroscopically observing the translational and rotational motion of solute molecules in liquid solutions is typically impeded by their interactions with the solvent, which conceal spectral detail through linewidth broadening. Here we show that unique insights into solute dynamics can be made when using perfluorinated solvents, which interact weakly with solutes and provide a simplified liquid environment that helps to bridge the gap in our understanding of gas and liquid phase dynamics. Specifically, we show that in such solvents, translational and rotational cooling of an energetic CN molecule can be observed directly using ultrafast transient absorption spectroscopy. We observe that translational energy dissipation within these liquids can be modeled through a series of classical collisions, whereas classically simulated rotational energy dissipation is shown to be distinctly faster than experimentally measured. We also observe the onset of rotational hindering from nearby solvent molecules, which arises as the average rotational energy of the solute falls below the effective barrier to rotation induced by the solvent.

Introduction:

In the gaseous phase, vibrational, rotational, and translational energy transfer between small molecules can be experimentally observed from time-dependent optical spectra. Vibrational and rotational state populations can be determined from the intensities and frequencies of rovibronic transitions, and the average translational energy can be determined from the Doppler broadening of the transition linewidths.[1] In the liquid environment, however, generally only vibrational state relaxation can be observed. Inhomogeneous spectral broadening, caused by varied and sizeable solvent-solute interactions, completely dominates the transition linewidths and conceals the narrowly spaced rotational transitions. Furthermore, interactions with the surrounding solvent typically prevent free molecular rotation, converting the interrupted angular motion into low frequency "librational" motion. Therefore, to observe translational and rotational motion in the liquid phase, the solvent molecules must be sufficiently non-interacting to minimize both inhomogeneous spectral broadening and rotational hindering.

Perfluorinated solvents such as perfluorohexane offer precisely such an environment. These solvents are known to hold large volumes of small gaseous molecules, a property exploited for liquid breathing applications popularized in science fiction films such as The Abyss and in the real-life treatment of Respiratory Distress Syndrome.[2] This property is linked to the presence of open cavities between the weakly interacting perfluorinated molecules, within which gas molecules can fit without significant disruption to the bulk liquid structure.[3] The weak intermolecular interactions induce only minor inhomogeneous broadening on the absorption spectra of molecules held within these cavities,[4] which are large enough to allow nearly unhindered molecular rotation for small molecules as shown in Supplementary Figure 1. Moreover, the solvents are completely unreactive, which eliminates

confuscating signal from unwanted side reactions with the solvent. The simplicity of the solvation combined with the large amounts of information contained within the structured spectra of solute molecules provides an ideal environment in which to study the dynamics of chemical reactions in solution. The influence of perfluorinated solvents on chemical reactions is limited to short-range collisional effects, and can therefore be treated as a simple perturbation to reactions that have been well-characterized in the gas phase. One such prototypical reaction, which we present here, is the ultraviolet photolysis of BrCN to liberate a Br atom and an energized CN radical.[5,6]

The CN photoproduct of deep-UV photolysis of ICN and BrCN is known to be produced with significant rotational excitation ($N_{max} > 50$).[5,7,8] For this reason, and because the CN fragment is easily probed with near-visible wavelengths, these systems have been the subject of extensive experimental and theoretical investigation in the gas and liquid phase.[9-20] Previous transient anisotropy measurements of ICN photolysis in liquid solutions performed by the Zewail[12] and Bradforth[13,14] groups observed that the CN photoproduct maintains a preferred plane of rotation for a few picoseconds after photolysis, presumed to be due to the gyroscopic stabilization of rapidly rotating CN fragments. This idea was supported by Molecular Dynamics (MD) simulations which observed the formation of a short–lived cavitation bubble in the solvent structure arising from the initial impact of the ballistic photofragments, within which the CN fragment could rotate relatively unhindered.[12-14] More recently, Rivera et al.[15] observed a large blue-shifting of the CN absorption signal after ICN photolysis in water solutions, taking place on a similar timescale to this loss of anisotropy. This shifting represents the transition of gas-like CN to solvated CN, and can only occur once the CN fragment has lost enough energy to complex with nearby water molecules. In each of these experiments, the CN rotational relaxation dynamics were probed indirectly since the rotational band structure cannot be resolved in conventional solvent environments. This limitation is overcome in the current study.
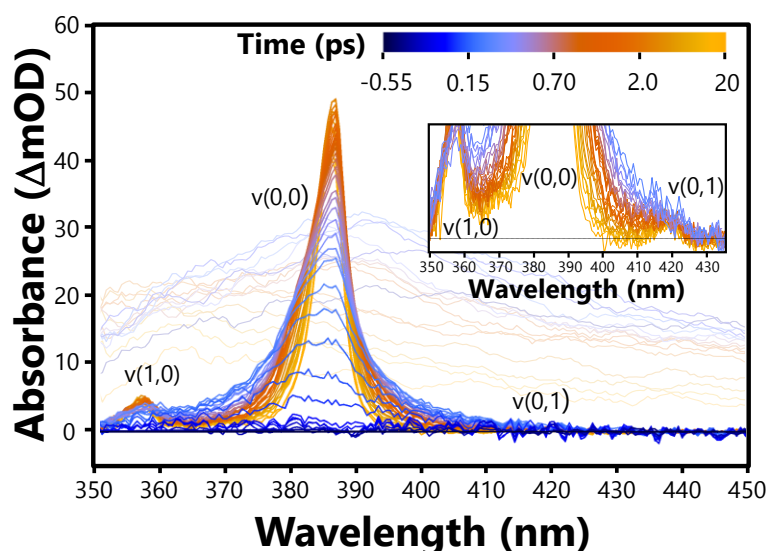
Results:
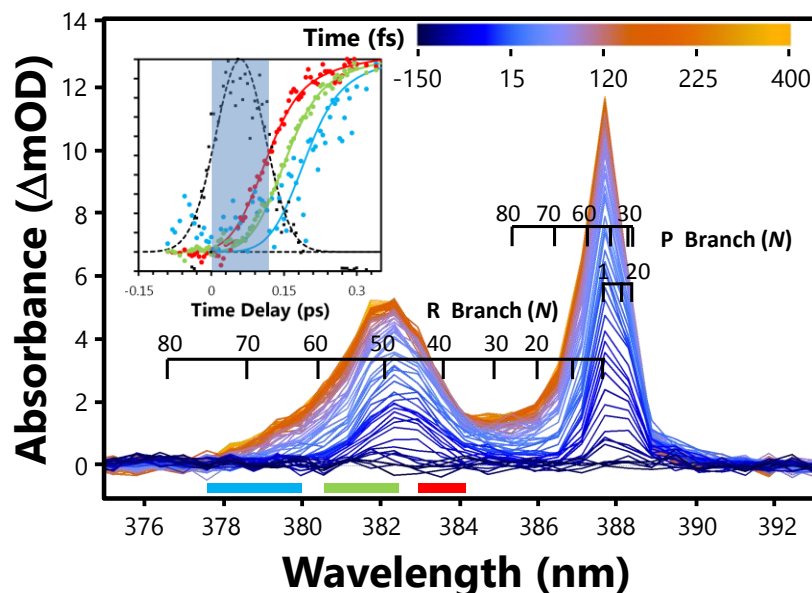
Figure 1 / Transient electronic absorption spectra resulting from gas phase BrCN photolysis at 220 nm: Spectra are shown at various time delays up to 400 fs after the photolysis laser pulse, and the absorption signal arises from the CN $B^2\Sigma^+$ ($v' = 0$, $N \pm 1$) $\leftarrow$ $X^2\Sigma^+$ ($v'' = 0$, N) transitions. The combs indicate the positions of P and R branch lines originating from different rotational levels N of ground state CN. Photofragment kinetic energies (and speeds) decrease as rotational excitation of the CN increases, so the lower rotational states of CN appear first. The colored kinetic traces in the inset show the integrated signal intensities as a function of pump-probe delay time for various spectral regions of the R branch

Figure 1 shows transient absorption spectra measured following the photolysis of gaseous BrCN at 220 nm. The features centered at 382.4 and 387.7 nm correspond to the R (ΔN = +1) and P ($\Delta N = -1$) rotational branches of the CN B $^2\Sigma^+$ (v' = 0) $\leftarrow$ X $^2\Sigma^+$ (v" = 0) transition. The band shapes demonstrate that the CN fragment is formed rotationally hot with a roughly Gaussian rotational state population distribution peaking near N = 50, consistent with the results of previous laser-induced fluorescence experiments.[5] Because of the infrequency of molecular collisions in the gas phase, we do not observe significant rotational relaxation in this distribution on the timescale of our measurement (up to 1.4 ns). The CN absorption grows to half of its maximum intensity about 120 fs after the BrCN parent absorbs the pump photon but this timescale depends on the rotational energy of the CN product fragment, with high N fragments delayed by up to a further 80 fs from the lower N fragments. These delays arise as a consequence of variations in the dissociative potential surfaces leading to the different N products, and because energy conservation constrains the recoil speeds to reduce as CN rotational excitation increases.[6]

Figure 2 / Transient electronic absorption spectra resulting from BrCN photolysis at 220 nm in perfluorohexane (foreground) and acetonitrile (background, vertically scaled by ×10) solutions: The spectra in acetonitrile are inhomogeneously broadened and contain obfuscating contributions from fragment charge transfer transitions. Spectra in perfluorohexane exhibit far less broadening and are composed *only* of CN B (v') $\leftarrow$ X (v") transitions labelled as v(v',v"). The inset shows a magnified portion of the spectra, where the v(0,1) transition arising from vibrationally excited CN X is clearly visible. The non-interacting perfluorohexane solvent allows us to extract solute translational, rotational, and vibrational dynamics from spectral details that are concealed by spectral line broadening in conventional solvents.

Figure 2 shows two transient absorption spectra arising from the 220 nm photolysis of BrCN in solution. The faded background shows the broadened spectra observed in acetonitrile. Although a recognizable CN feature near 388 nm is observable during the first picosecond after dissociation of BrCN in acetonitrile, it is too broad to resolve any information about the populated CN quantum states. In contrast, the transient spectra in perfluorohexane (Figure 2 foreground) are vibronically resolved into distinct CN B (v') $\leftarrow$ X (v") transitions, showcasing the non-interacting nature of the solvent. Close inspection of the baseline (Figure 2 inset) reveals the isolated B (v' = 0) $\leftarrow$ X (v" = 1) transition, consistent with the minor yield of CN X (v" = 1) observed in collision-free gas-phase spectra.[5] The v" = 1 population decays negligibly over the timescale of our experiment (1.4 ns), indicating a

vibrational relaxation time >5 ns. Because the CN transitions are sharper in the perfluorinated environment, the temporal evolution of their lineshapes can be clearly observed, revealing information about the chemical dynamics of the system.

Discussion:

The CN B ← X lineshape evolves from an initially broad (>1000 cm^{-1} full width at half maximum linewidth, Figure 3) Lorentzian profile to a much narrower (240 cm^{-1}) near-Gaussian profile. Gaussian lineshapes indicate inhomogeneous broadening typical of the non-uniform liquid environment, while Lorentzian lineshapes indicate homogeneous broadening originating from dynamic motion. Frequent molecular collisions cause homogenous broadening of spectral lines following from the energy-time uncertainty principle, since perturbing intermolecular forces decrease the dephasing time of the transition. The narrowing of the Lorentzian contribution to the linewidth therefore represents the loss of kinetic energy of the translationally and rotationally hot CN photofragments through successive encounters with the surrounding solvent molecules.

The observed early time Lorentzian linewidth, Γ, implies a <5 fs dephasing time for the B ← X transitions of the newborn CN fragment. In a simple impact-limited model of collisional broadening, the dephasing time is equal to the time between molecular collisions. However, when the collisional duration approaches the time between collisions, a quasi-static model incorporating the interaction potential of the colliding molecules must be utilized instead.[21,22] A notable expectation of quasi-static broadening theory is the introduction of asymmetric lineshapes, since the energy levels of the probed molecule are perturbed by the collisional interaction potential for a significant fraction of the time. We observe a noticeable wing on the short wavelength side of the transition, consistent with the destabilization of the diffuse CN B electronic state by a primarily repulsive interaction potential with the perfluorocarbon solvent.
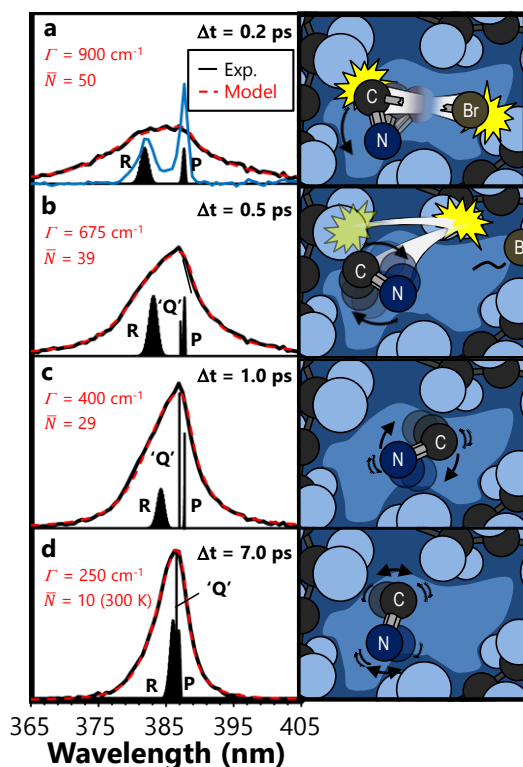
Figure 3 / Interpretation of transient spectra from Figure 2: Selected transient spectra are shown of the CN X (v" = 0) products from BrCN photolysis in perfluorohexane at 220 nm, along with the results of our best fit model and line spectra of the simulated underlying rotational distribution used in the model (black solid).[23] Panel (a) also overlays the transient gas phase spectrum from Figure 1 (blue solid) for comparison. The model is the sum of P, Q, and R branch components with time-varying Γ and $\bar{N}$ values, but static Gaussian linewidths of 240 cm^{-1} and a Q:P/R intensity ratio defined by Equation 1. (a) The CN fragment is generated with hyperthermal translational and rotational energy ($\bar{N}$ = 50). (b) The homogeneous linewidth of the absorption spectrum narrows as translational energy dissipates and perturbing interactions with the solvent become less frequent. (c-d) As the rotational energy is lost, a solvent induced rotational barrier hinders the angular motion of the CN molecule, converting rotational motion into pendular librational motion and the P/R rotational branches into a pure vibrational transition (a false 'Q'-branch). See Supplemental Movie 1 for an animation of the experimental and decomposed model spectra at all time delays.

The rotational excitation of the CN photofragment can be directly observed from the positions of the P and R branch transitions in the spectrum (comb in Figure 1). Although the P and R branch peaks are not completely resolved in the solution-phase spectra, they are still evident as shoulders in the spectral lineshapes and show the same level of initial rotational excitation as the gas-phase spectra (Figure 3a). Because the transition linewidth is wider than the spread of transition energies spanned by the initial rotational distribution, only the average CN rotational quantum number $\bar{N}$ is required to model the spectrum. The transition linewidth and the apparent widening of the lineshape due to underlying rotational excitation have easily separable contributions to our model, since rotational excitation broadens the lineshape toward shorter wavelengths only (see rotational combs in Figure 1) and the transition linewidth broadens symmetrically (and with distinct Lorentzian tails). The P and R branches converge as the CN rotation thermalizes. The branch centers can be distinguished down to about $\bar{N}$ = 22 ($\bar{E}_{rot}(\bar{N})$ = 960 cm^{-1}), between panels (c) and (d) of Fig. 3, when the spacing between the P and R features becomes comparable to the transition linewidth.

Figure 4 shows the time-dependent evolution of the Lorentzian linewidth and average rotational energy extracted from the experimental spectra. The Lorentzian linewidth narrows mostly within the first picosecond after photolysis, while the rotational energy cools over twice as slowly. The rotational relaxation timescale of several picoseconds is comparable to those inferred previously from transient anisotropy experiments in other solvents.[13,14] Also

plotted in Figure 4 are the corresponding results of MD simulations performed on a CN fragment, instantaneously provided with the experimental recoil velocity of 30 Å/ps and rotational energy corresponding to $N = 50$, in a solution of perfluorohexane (80 molecules in a 30 Å periodic box, microcanonical simulation). We find a remarkable correlation between the experimental Lorentzian linewidth and the CN fragment velocity extracted from the simulation, which results from the transition dephasing rate of the CN fragment being proportional to the speed with which it experiences different interactions with the solvent. The time-dependent correlation implies that the translational cooling can be well-described by classical dynamics. The MD simulations predict a similar timescale for translational and rotational cooling which significantly overestimates the rotational relaxation rate observed experimentally. This discrepancy may imply that rotational energy transfer is limited by the quantization of rotational states, but we interpret these results cautiously since the simulated relaxation rates are strongly dependent on the chosen values of interaction potential parameters.

The spectral lineshape is observed to continue evolving on a slower timescale, reaching its final equilibrated shape ~10 ps after the CN fragment is generated. This behavior is best captured in our model by a further narrowing of the Lorentzian linewidth over this time period however, after ~2 ps, the homogeneous, inhomogeneous, and rotational band contributions to the lineshape are difficult to distinguish. We attribute this slower linewidth evolution to the thermalization of the nearby perfluorohexane molecules. The large quantity of translational and rotational energy contained within the initially hot CN fragment must be transferred to the solvent, resulting in a surrounding shell of hot solvent molecules. This non-equilibrated solvent shell will delay the thermalization of the last portion of excess CN translation and rotational energy.
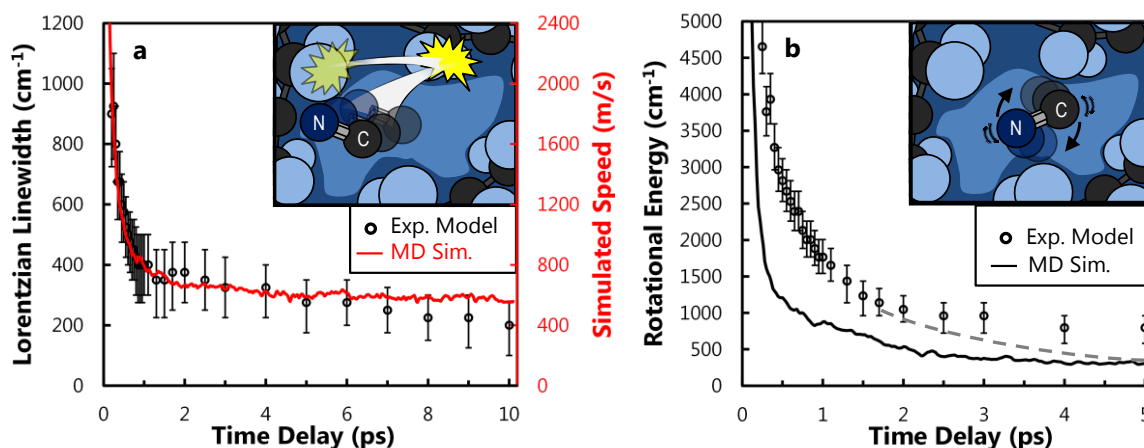
Figure 4 / Kinetic traces of translational and rotational energy relaxation: (a) Evolution of the Lorentzian linewidth of the CN B ← X transition obtained from the experiment, compared with the average CN speed extracted from the MD simulations. The faster moving CN fragment experiences more frequent changes in interaction with the solvent, leading to the observed relationship between these values. (b) Evolution of the average rotational energy obtained from the experimental spectra, compared to the average rotational energy extracted from the MD simulations. The average rotational energy must eventually approach the 300 K thermal average of 208 cm^{-1}, but the spectral decomposition after 2 ps becomes ambiguous and does not capture this trend. The dashed grey line suggests what the CN rotational energy may look like after this time. The upper and lower limits of the experimental error bars were obtained by increasing or decreasing the relevant model parameter (Γ or $\bar{N}$) until the sum of square residuals between the model and experimental spectra doubled in value. Although the translational energy relaxation is well captured by our MD simulations, the simulated rotational energy relaxation is significantly faster than experimentally observed.

A subtle peak grows in the spectral profile consistent with the wavelength for the rotationless CN B ($v' = 0$) ← X ($v'' = 0$) vibronic transition, and is reminiscent of a Q-branch,

although only P and R branch transitions are allowed for a Σ–Σ transition in the gas-phase. Although this peak is not fully resolved, its contribution to the observed lineshape cannot be captured by any realistic evolution of the P and R branch basis functions alone (see Supplementary Figure 2). This false "Q-branch" arises from rotational hindering induced by the surrounding solvent molecules.[24-26] If rotation is sufficiently hindered, N is no longer a good quantum number and the spectrum collapses to a pure vibrational spectrum. The degree to which molecular rotation is hindered in solution can therefore be measured by the ratio of P/R to 'Q' branch intensities in the absorption spectrum. This solvent hindering becomes significant as the average rotational energy relaxes below the average height of the hindering barrier. In our model of the experimental spectra, a satisfactory fit is obtained if the ratio of P/R to 'Q' branch intensities, denoted by $P_{rot}(\overline{N})$, is linked to the CN rotational cooling through an Arrhenius-like expression representing the likelihood of passing over the rotational barrier:

$$P_{rot}(\overline{N}) \propto \exp\left(-\frac{E_{barrier}}{\overline{E}_{rot}(\overline{N})}\right) \qquad (1)$$

where $P_{rot}(\overline{N}) = 1$ indicates free rotation with a spectrum composed of only P and R branches, and $P_{rot}(\overline{N}) = 0$ indicates completely hindered rotation and a pure 'Q'-branch spectrum. Fitting to this expression, we obtain a rotational barrier height, $E_{barrier} = 500$ cm⁻¹. This onset of solvent hindering also induces a 145 cm⁻¹ shift in the spectral transitions towards higher frequencies, similar to that observed in the spectra of molecules tightly confined in rare-gas matrices.[27]

This rotational barrier model is a more general interpretation of the 'cavitation bubble' model proposed by Stratt and coworkers based on simulations of ICN photolysis in liquid argon.[13] The initial collision of the CN (N=37) with the argon displaced the surrounding solvent atoms to generate a small open bubble in the solvent, within which the CN freely rotated until the solvent relaxed around it. Perfluorohexane is not as easily displaced as argon, and our MD simulations do not reveal any significant expansion of the initial solvent cavity within which the CN fragment resides (Supplementary Figure 3). This implies that the initial generation of a short-lived solvent cavity is not necessary for the observation of solute rotation, so long as the solute is sufficiently rotationally energetic.

Conclusion:

The story of BrCN photolysis in perfluorohexane solution, as interpreted from the results presented here, is thus summarized as follows: 120 fs after the absorption of a 220 nm photon, the Br-CN bond is fully broken and the CN(X) photofragment is ejected into the solvent with a maximum recoil speed of 30 Å/ps, an average rotational quantum number of 50, and mostly vibrationally unexcited. The translational energy is largely dissipated within the first picosecond after dissociation. The majority of the rotational energy is dissipated within 2 picoseconds, approximately twice as slowly as classical trajectories predict. As the rotational energy falls below the barrier arising from obstructing solvent molecules, the initially free CN rotation is converted to interrupted librational motion. The large amount of CN translational and rotational energy is absorbed by the surrounding solvent molecules, resulting in a locally hot solution which equilibrates with the bulk over the next 10 ps. Vibrational excitation of the CN persists for at least several nanoseconds. The interactions of the equilibrated CN fragment with the perfluorocarbon solvent are dominated by short range repulsion, which leads to modest inhomogeneous broadening of the solute spectrum on the order of 240 cm⁻¹.

Perfluorocarbon solvents afford a liquid environment in which the photodissociation and the subsequent equilibration of the photofragments can be observed with resolution of

translational, rotational and vibrational dynamics. The solvents provide a simplified approach towards unravelling the immensely complicated chemical dynamics of the bulk liquid phase.

Methods:

Transient Spectroscopy: BrCN was photolyzed using a UV pump pulse with a wavelength of 220 nm. The pump pulses were delivered to the liquid samples at repetition rates reduced to half the probe pulse frequency of 1 kHz using a mechanical chopper in order to obtain pump on/pump off difference spectra. Less than 1 μJ/pulse of the fundamental output of an amplified Titanium:Sapphire laser (1 kHz, 40 fs pulse duration) was focused into a rastered 5-mm thick CaF_2 window using a 100-mm focal length lens to generate the white-light continuum probe pulse. The recollimated probe pulses spanned the approximate wavelength range of 330 to 800 nm, and were overlapped spatially with the UV pulses at the sample to sub 200 μm focal diameters. For the gas-phase measurements, the pump and probe pulses were gently focused with a 500 mm focal length lens and propagated nearly collinearly to maximize overlap within the entire 10 cm gas cell. A motorized stage varied the length of the path followed by the UV laser pulses to set the time delays between pump and probe pulses. Delays were selected between −1 and +1300 ps with time steps as small as 5 fs.   The transmitted probe light was collected into an optical fiber and dispersed onto a 750-pixel CCD spectrometer (Avantes, AvaSpec-DUAL) with a spectral resolution of 0.6 nm. The baseline of the spectrum shows a minor offset caused by a coherent artifact when the pump and probe laser pulses are overlapped in time, providing a convenient internal reference of time zero and the instrument response function, which can be well modeled by a Gaussian temporal profile with a full-width at half maximum of 120 fs.

Sample Preparation: Liquid phase transient electronic absorption spectroscopy measurements were conducted with solutions of BrCN (Aldrich; 97 %) which were prepared in perfluorohexane (Aldrich; 99 %) and distilled acetonitrile. Perfluorohexane underwent >3 freeze-pump-thaw cycles with liquid nitrogen to remove dissolved gas from the solvent before solid BrCN crystals were deposited in the solution. Sample volumes of 10 ml were circulated through a PTFE optical flow cell (500 μm path length), fitted with CaF_2 windows, using a peristaltic pump and PTFE tubing. The gas-phase measurements of BrCN were obtained by placing a few crystals of BrCN in a 10 cm long pyrex optical cell with CaF_2 windows.

MD Simulations: The Optimized Potentials for Liquid Simulations All Atoms (OPLSAA) [28-30] force field was used to carry out liquid phase simulations. Since there were no force field parameters for the CN radical, the generic alkyl CN (Atom types: 692 and 691 respectively) parameters were chosen instead in the present work. The Tinker suite of codes was used to perform MD calculations. A periodic box with a length of 30 Å was filled with 80 perfluorohexane molecules. The energy of the box was subsequently minimized by adjusting the geometry of the molecules. A CN radical was placed in the centre of mass of the box, the energy of which was again minimized. The system was equilibrated for 5 ps with a time step of 0.5 fs at a temperature of 298 K under NVT conditions. The CN molecule in the simulation box was then replaced by another one which was initialised in the following way. The CN vibration was approximated by a harmonic oscillator whose force constant matched the experimental vibrational wavenumber of 2068 cm^{-1}, and the CN molecule was set to its zero-point energy of 1034 cm^{-1}. The vibrational phase of the CN radical was set randomly. The initial rotational quantum number of the radical was set to 50. Its centre-of-mass velocity had a magnitude of 30 Å ps^{-1} and an orientation identical to the final velocity of the CN radical from the NVT simulation. The center-of-mass of the prepared CN radical was moved

to that of the CN radical found at the end of NVT simulation. The simulation was propagated for 10 ps using a timestep of 0.1 fs under NVE conditions. The Velocity-Verlet algorithm was employed to propagate the trajectories both in the NVT and NVE simulations. The conservation of energy was better than 4 parts per million (0.0023 kJ mol^{-1} at a mean total energy of 690 kJ mol^{-1}). 200 simulations were accumulated to obtain statistically relevant results. The simulated kinetic traces are offset from zero by 120 fs, to account for the experimentally observed Br−CN bond-breaking time.

References and Notes:

1   Demtröder, W. *Laser Spectroscopy*. 4th edn, (Springer, 2008).
2   Leach, C. L. *et al.* Partial liquid ventilation with perflubron in premature infants with severe respiratory distress syndrome. *New Engl. J. Med.* **335**, 761-767 (1996).
3   Riess, J. G. Understanding the fundamentals of perfluorocarbons and perfluorocarbon emulsions relevant to in vivo oxygen delivery. *Artif. Cell Blood Sub.* **33**, 47-63 (2005).
4   Myers, A. B. & Li, B. L. Resonance Raman Quantum Yields for CS_2 in Solution - Dynamics of Solvent-Induced Spectral Broadening. *J. Chem. Phys.* **92**, 3310-3322 (1990).
5   Fisher, W. H. *et al.* Photodissociation of BrCN and ICN in the A Continuum - Vibrational and Rotational Distributions of CN($X^2\Sigma^+$). *Chem. Phys.* **89**, 457-471 (1984).
6   Huang, C. S., Li, W., Silva, R. & Suits, A. G. DC slice ion imaging of the ultraviolet photodissociation of BrCN. *Chem. Phys. Lett.* **426**, 242-247 (2006).
7   Halpern, J. B. & Jackson, W. M. Partitioning of Excess Energy in the Photolysis of Cyanogen Chloride and Cyanogen-Bromide at 193 nm. *J. Phys. Chem.* **86**, 3528-3533 (1982).
8   Nadler, I., Reisler, H. & Wittig, C. Energy Disposal in the Laser Photodissociation of ICN and BrCN at 300 K and in a Free Jet Expansion. *Chem. Phys. Lett.* **103**, 451-457 (1984).
9   Dantus, M., Rosker, M. J. & Zewail, A. H. Femtosecond Real-Time Probing of Reactions. II. The Dissociation Reaction of ICN. *J. Chem. Phys.* **89**, 6128-6140 (1988).
10   Dantus, M., Bowman, R. M., Baskin, J. S. & Zewail, A. H. Femtosecond Real-Time Alignment in Chemical Reactions. *Chem. Phys. Lett.* **159**, 406-412 (1989).
11   Benjamin, I. & Wilson, K. R. Proposed Experimental Probes of Chemical Reaction Molecular Dynamics in Solution: ICN Photodissociation. *J. Chem. Phys.* **90**, 4176-4197 (1989).
12   Wan, C. Z., Gupta, M. & Zewail, A. H. Femtochemistry of ICN in liquids: Dynamics of dissociation, recombination and abstraction. *Chem. Phys. Lett.* **256**, 279-287 (1996).
13   Moskun, A. C., Jailaubekov, A. E., Bradforth, S. E., Tao, G. H. & Stratt, R. M. Rotational coherence and a sudden breakdown in linear response seen in room-temperature liquids. *Science* **311**, 1907-1911 (2006).
14   Moskun, A. C. & Bradforth, S. E. Photodissociation of ICN in polar solvents: Evidence for long lived rotational excitation in room temperature liquids. *J. Chem. Phys.* **119**, 4500-4515 (2003).
15   Rivera, C. A., Winter, N., Harper, R. V., Benjamin, I. & Bradforth, S. E. The dynamical role of solvent on the ICN photodissociation reaction: connecting experimental observables directly with molecular dynamics simulations. *Phys. Chem. Chem. Phys.* **13**, 8269-8283 (2011).
16   Winter, N., Chorny, I., Vieceli, J. & Benjamin, I. Molecular dynamics study of the photodissociation and photoisomerization of ICN in water. *J. Chem. Phys.* **119**, 2127-2143 (2003).
17   Benjamin, I. Photodissociation of ICN in Liquid Chloroform - Molecular-Dynamics of Ground and Excited-State Recombination, Cage Escape, and Hydrogen Abstraction Reaction. *J. Chem. Phys.* **103**, 2459-2471 (1995).
18   Johnson, M. L. & Benjamin, I. Photodissociation of ICN at the Water/Chloroform Interface. *J. Phys. Chem. A* **113**, 7403-7411 (2009).
19   Vieceli, J., Chorny, I. & Benjamin, I. Photodissociation of ICN at the liquid/vapor interface of chloroform. *J. Chem. Phys.* **115**, 4819-4828 (2001).
20   Winter, N. & Benjamin, I. Photodissociation of ICN at the liquid/vapor interface of water. *J. Chem. Phys.* **121**, 2253-2263, doi:10.1063/1.1765093 (2004).
21   Chen, S. Y. & Takeo, M. Broadening and Shift of Spectral Lines Due to the Presence of Foreign Gases. *Rev. Mod. Phys.* **29**, 20-73 (1957).
22   Bambini, A., Berman, P. R., Buffa, R., Robinson, E. J. & Matera, M. Laser-Induced Collisional Energy-Transfer. *Phys. Rep.* **238**, 245-339 (1994).

23   Western, C. M. PGOPHER: A program for simulating rotational, vibrational and electronic spectra. *J. Quant. Spectrosc. Radiat. Transfer* **In Press**, doi:10.1016/j.jqsrt.2016.04.010 (2016).

24   Talin, B., Galatry, L. & Klein, L. Relaxation Processes and Spectra in Liquids and Dense Gases. *J. Chem. Phys.* **66**, 2789-2800 (1977).

25   Robert, D. & Galatry, L. Calculation of infrared band shapes in liquid solutions of diatomic polar molecules in nonpolar solvents. *Chem. Phys. Lett.* **1**, 399-403 (1967).

26   Padilla, A., Perez, J., Herrebout, W. A., Van der Veken, B. J. & Bulanin, M. O. A simulation study of the vibration-rotational spectra of HCl diluted in Ar: Rotational dynamics and the origin of the Q-branch. *J. Mol. Struct.* **976**, 42-48 (2010).

27   Thoma, A., Schallmoser, G., Smith, A. M., Wurfel, B. E. & Bondybey, V. E. Visible Absorption and Infrared-Emission of CN-Xe in an Argon Matrix. *J. Chem. Phys.* **100**, 5387-5389 (1994).

28   Jorgensen, W. L. & Tirado-Rives, J. The OPLS Potential Functions for Proteins - Energy Minimizations for Crystals of Cyclic-Peptides and Crambin. *J. Am. Chem. Soc.* **110**, 1657-1666 (1988).

29   Jorgensen, W. L., Maxwell, D. S. & Tirado-Rives, J. Development and testing of the OPLS all-atom force field on conformational energetics and properties of organic liquids. *J. Am. Chem. Soc.* **118**, 11225-11236 (1996).

30   Watkins, E. K. & Jorgensen, W. L. Perfluoroalkanes: Conformational analysis and liquid-state properties from ab initio and Monte Carlo calculations. *J. Phys. Chem. A* **105**, 4118-4125 (2001).

Author Contributions: M.P.G., A.J.O.E. and M.N.R.A. conceived the study. M.P.G., P.M.C. and R.S.M. planned and performed the liquid-phase transient experiments. H.J.B.M. planned and performed the transient gas-phase experiments. M.P.G. and P.M.C. analyzed the data and conceived the theoretical models. B.H. performed the Molecular Dynamics simulations. M.P.G., A.J.O.E. and M.N.R.A. wrote the paper with input from all authors.

Additional information: Supplementary information is available in the online version of the paper. Reprints and permissions information is available online at www.nature.com/reprints. Correspondence and requests for materials should be addressed to M.P.G.

Competing financial interests: The authors declare no competing financial interests.